

Effects of mountains on aerosols determined by AERONET/DRAGON/J-ALPS measurements and regional model simulations

Makiko Nakata¹, Mizuo Kajino², and Yousuke Sato³

¹Kindai University

²Meteorological Research Institute

³Hokkaido University

November 23, 2022

Abstract

The NASA/AERONET field campaign DRAGON/J-ALPS (Distributed Regional Aerosol Gridded Observation Networks/Joint work to the Aerosol Properties and Process Simulations) was conducted from March 2020 to May 2021 in Nagano, Japan. Twelve sun photometers were installed around Nagano prefecture. The effects of topography on aerosols were studied using observations and simulations. In this study, a regional chemical transport model (SCALE-Chem) was employed. Three numerical experiments were conducted: E1 (control experiment), E2 (E1 without topography), and E3 (E1 with removal of all anthropogenic emissions over Nagano prefecture). In E2, the terrain effect was not considered; the difference between E1 and E2 indicated the influence of mountains. The differences between E1 and E3 evaluate the local emission effect. In some cases, the mountainous terrain seemed to have suppressed aerosol inflow (i.e., reduced aerosol concentration), while in other cases, the mountains contributed to aerosol retention on days when aerosols tended to accumulate in mountain basins due to local emissions. Thus, while mountains prevent the inflow of aerosols from outside, they also contribute to increased aerosol concentration in the basin. Naturally, more significant effects are produced by meteorological conditions and the presence or absence of transboundary pollution from the outside. From observations and model simulations, we found that the aerosol concentration was not high around the J-ALPS site because of the mountain effect that prevents advection from the outside, even when transboundary pollution was observed in Japan in March 2020.

18 **Abstract**

19 The NASA/AERONET field campaign DRAGON/J-ALPS (Distributed Regional Aerosol
20 Gridded Observation Networks/Joint work to the Aerosol Properties and Process Simulations)
21 was conducted from March 2020 to May 2021 in Nagano, Japan. Twelve sun photometers were
22 installed around Nagano prefecture. The effects of topography on aerosols were studied using
23 observations and simulations. In this study, a regional chemical transport model (SCALE-Chem)
24 was employed. Three numerical experiments were conducted: E1 (control experiment), E2 (E1
25 without topography), and E3 (E1 with removal of all anthropogenic emissions over Nagano
26 prefecture). In E2, the terrain effect was not considered; the difference between E1 and E2
27 indicated the influence of mountains. The differences between E1 and E3 evaluate the local
28 emission effect. In some cases, the mountainous terrain seemed to have suppressed aerosol
29 inflow (i.e., reduced aerosol concentration), while in other cases, the mountains contributed to
30 aerosol retention on days when aerosols tended to accumulate in mountain basins due to local
31 emissions. Thus, while mountains prevent the inflow of aerosols from outside, they also
32 contribute to increased aerosol concentration in the basin. Naturally, more significant effects are
33 produced by meteorological conditions and the presence or absence of transboundary pollution
34 from the outside. From observations and model simulations, we found that the aerosol
35 concentration was not high around the J-ALPS site because of the mountain effect that prevents
36 advection from the outside, even when transboundary pollution was observed in Japan in March
37 2020.

38

39 **Plain Language Summary**

40 Aerosol observations by the NASA/AERONET field campaign were conducted in the
41 mountainous regions of Japan from March 2020 to May 2021. This field campaign is called
42 DRAGON/J-ALPS because the target area includes the mountains known as the Japanese Alps.
43 In this study, we investigated how mountains affect aerosol distribution by using simulations
44 with the regional chemical transport model SCALE-Chem in conjunction with observational data
45 in mountainous regions. To investigate the effect of mountains, simulations were conducted with
46 and without mountains. In addition, to investigate the effect of local sources, we compared
47 simulations with and without anthropogenic emissions in the target area. The simulation results
48 showed that the mountains blocked aerosols and created a basin effect by increasing the aerosol
49 concentration near the surface. Furthermore, averaged throughout March 2020, the effect of the
50 mountains blocking aerosols was greater than the effect of the mountains increasing aerosol
51 concentrations near the surface. This finding suggests that the blocking effect of the surrounding
52 mountains prevented an increase in aerosol concentrations at the J-ALPS site even on days when
53 transboundary pollution from mainland China arrived in Japan.

54

55 **1 Introduction**

56 Atmospheric aerosols are attracting attention not only as substances that affect the climate
57 (IPCC, 2013) but also as PM_{2.5}, which causes air pollution (Shinder et al., 2016, Van Donkelaar et
58 al., 2015). Because aerosols are not uniform and have a local spatio-temporal distribution, high
59 spatial resolution observations are very important. The AErosol RObotic NETwork project
60 (AERONET; Holben et al., 1998) is an international network of ground-based sun photometers

61 that provides atmospheric aerosol properties. The series of distributed regional aerosol gridded
62 observation network (DRAGON) campaigns began in 2011 as a relatively high spatial density of
63 ground-based sun photometers and other associated measurements of limited duration (Holben et
64 al., 2018). DRAGON field campaigns are conducted worldwide to provide high-resolution ground-
65 based data for remote sensing and model simulations.

66 The following two campaigns, DRAGON-KOREA and DRAGON-JAPAN, operated from
67 March to June 2012 to elucidate the aerosol characteristics of urban areas in East Asia where
68 transboundary and urban pollution are mixed. During DRAGON-KOREA in Seoul, it was
69 observed that industry and fossil fuel power generation contributed emissions to a significant
70 pollution aerosol loading in addition to aerosols transported from mainland China. DRAGON-
71 JAPAN was held mainly in Osaka during the DRAGON-KOREA campaign. In Osaka, small
72 particles emitted from factories are dominant, but when yellow dust particles are introduced, the
73 percentage of large particles increases (Nakata et al., 2015). Further measurements with a mobile
74 sun photometer attached to a car showed that aerosol concentrations rapidly changed in time and
75 space over most of the Osaka area (Sano et al., 2016). Thus, the East Asian region has been
76 suffering from the effects of air pollution, much of which is transboundary. The extant literature
77 reports a significant impact of transboundary air pollution in Japan (Aikawa et al., 2010; Kaneyasu
78 et al., 2014; Nakata et al., 2015). Therefore, when considering the distribution of atmospheric
79 aerosols in Japan, it is necessary to consider not only aerosols of local origin but also transboundary
80 aerosols. Past DRAGON campaigns in Japan have focused on large urban areas and areas
81 susceptible to transboundary pollution. How do aerosols behave in mountainous areas with
82 complex topography? It has been reported that the mountainous areas of the Alps, where one would
83 expect a clean air environment, are surprisingly polluted as pollutants emitted from the
84 surrounding areas are carried by the wind through the valleys (Diemoz et al., 2019). Inspired by
85 this report, DRAGON-JALPS was designed to observe the effects of mountain topography on
86 aerosols in the mountainous areas of Japan.

87 Air pollutant emissions are the primary driver of the increase in aerosol concentration, and
88 meteorological conditions play a major role in exacerbating air pollution (Hu et al., 2020). Because
89 topography has a considerable effect on the meteorological conditions in the area, a study of the
90 local terrain associated with weather patterns and pollutant transport is important (Chuang et al.,
91 2008). The effects of topography on aerosol concentrations in East Asia have also been studied.
92 The Sichuan Basin in Southwest China has frequent heavy pollution, and the topographic effects
93 intensify haze pollution by reducing wind speed and varying air temperature and humidity in the
94 lower troposphere (Shu et al., 2020; Zhang et al., 2019). A study of the Twain-Hu basin in Central
95 China has shown that the basin topography plays an important role in the significant increase in
96 PM_{2.5}, although the meteorology altered by topography can alleviate local PM_{2.5} pollution over the
97 basin (Hu et al., 2020). The simulation results show that topography has a considerable influence
98 on haze pollution in Beijing (Zhang et al., 2018) and Taipei (Chuang et al., 2008).

99 The area around the Japanese Alps, which is the focus of this study, has a lower
100 concentration of atmospheric aerosols than Osaka, which is also in Japan. We hypothesize that this
101 may be due to the effect of the surrounding high mountains that mitigate transboundary pollution.
102 The issue of transboundary pollution, where polluted air from Tokyo, a large city located east of
103 Nagano Prefecture, travels over mountain passes and is transported to mountainous areas, has been
104 dealt with observations and models (Chang et al., 1989; Sasaki et al., 1988). However,
105 transboundary pollution from Tokyo is mainly observed in the summer season, and there are few

106 cases in the spring season, which is the target of this study. Rather, spring is the time when
107 transboundary pollution from the Chinese mainland is most likely to occur. Therefore, the main
108 objective of this study is to investigate the effect of mountains on long-distance transboundary
109 pollution by taking advantage of the opportunity of the intensive field campaign of J-ALPS. We
110 will clarify how the mountains affect the aerosol concentration by using ground-based observation
111 data during the DRAGON-JALPS field campaign and simulated by a chemical transport model.

112 **2 Materials and Methods**

113 2.1 AERONET field campaign: J-ALPS

114 2.1.1 Target area

115 Nagano Prefecture, the target area of J-ALPS, is located at the center of Japan's main island
116 and surrounded by mountains over 2000 m with multiple basins. These basins are located at
117 altitudes of 350–700 m, and some of them are connected to each other by major rivers. The
118 headwaters of all the major rivers are located in the prefecture, and because some head to the Sea
119 of Japan and others to the Pacific Ocean, the area around some of the headwaters is a watershed in
120 the central part of the main island of Japan. From the northwest to the south of the prefecture, there
121 are three mountain ranges: the Hida, Kiso, and Akaishi Mountains, collectively known as the
122 Japanese Alps (Togashi, 2001). The Hida, Kiso, and Akaishi Mountains are sometimes referred to
123 as the Northern, Central, and Southern Japanese Alps, respectively.

124 Geographic information on the location and elevation of each J-ALPS site is shown in Fig.1
125 and Table 1. The altitude of each site is the height of the location where the sun photometer is
126 installed. Both the Hakuba and Omachi sites are located in the northwestern part of Nagano
127 Prefecture, at the foot of the Northern Japanese Alps, with mountains around 3,000 m high on the
128 west side and mountains around 1,500 m high on the east side. Omachi city is to the south of
129 Hakuba, as shown in Fig.1. The climate of both sites is cool in summer and cold in winter, with
130 abundant snowfall. Matsumoto is a city with 200,000 people located slightly west of the center of
131 Nagano Prefecture, in the middle of the Matsumoto Basin between two mountain ranges. The
132 climate is characterized by diurnal and annual temperature differences, little precipitation, and
133 many sunny days. Suwa is located in central Nagano Prefecture, bordered by Lake Suwa to the
134 northwest and sandwiched between mountains to the west and east, roughly in the center of the
135 Suwa Basin. The climate in Suwa is characterized by more precipitation in spring, summer, and
136 autumn and far less precipitation in winter. The Minowa site is located in Minami-Minowa village
137 in the southern part of Nagano Prefecture, and the Ina site is situated in Ina city in the south.
138 Minowa and Ina lie in the northern part of the Ina Basin, with the Southern Japanese Alps to the
139 east, the Central Japanese Alps to the west, and the Tenryū River running through the center of the
140 basin. Iida is located in the southernmost part of Nagano Prefecture. The Iida basin, characterized
141 by terraces developed on both sides of the Tenryū River and the fans formed by its tributaries, has
142 a mild climate and relatively flat surfaces.

143

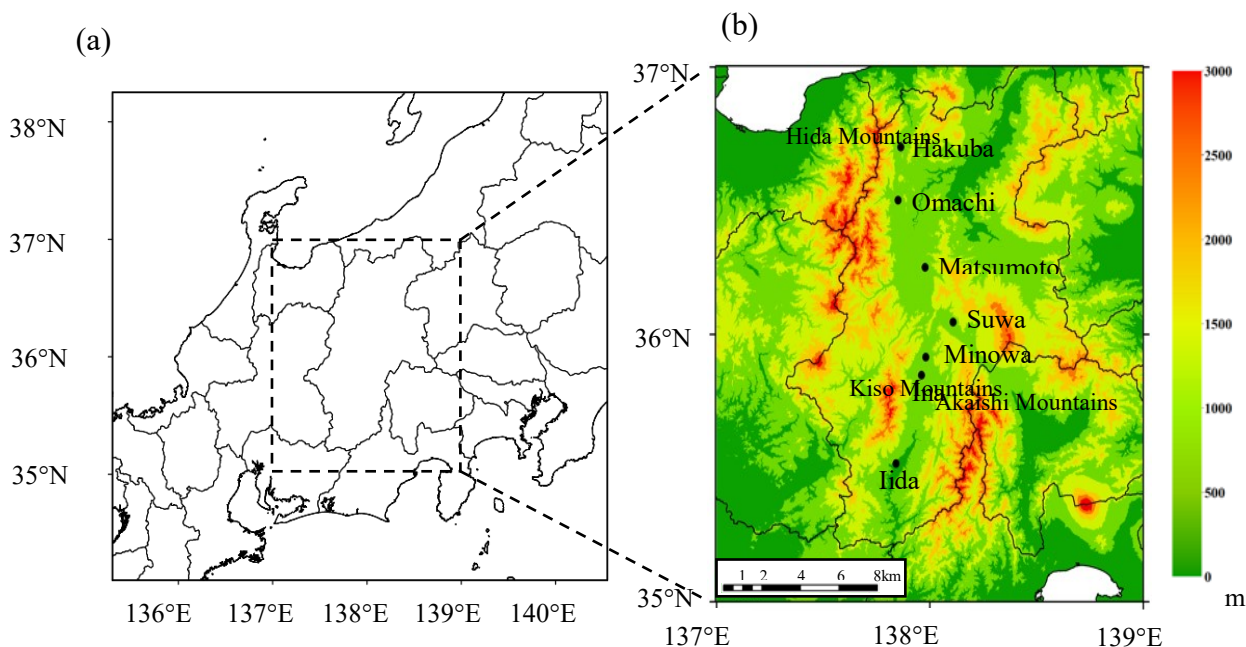
144

145

146

147

148



149

150 **Figure 1.** Geographic information of the model simulation (a) and the observation station of J-
 151 ALPS (b). The color scale on the right side denotes the elevation in meters.

152

153

Table 1. Specific geographic information of J-ALPS observation.

Site name	Latitude (degree)	Longitude (degree)	Altitude (m)
Hakuba	N 36.701	E 137.864	703
Omachi	N 36.503	E 137.851	751
Matsumoto	N 36.251	E 137.978	626
Suwa	N 36.046	E 138.109	766
Minowa	N 35.915	E 137.981	713
Ina	N 35.848	E 137.961	683
Iida	N 35.517	E 137.842	490

154

155

156

2.1.2 Measurements

157 A Cimel electric sun photometer was installed at each site in Fig.1 in March 2020. Sun
 158 photometer measurements of direct solar radiation provide information for calculating the
 159 columnar aerosol optical thickness (AOT). Aerosol optical thickness can be used to compute
 160 columnar water vapor and estimate the aerosol size distribution using the Ångström exponent
 161 relationship. We used version 3 of the AERONET database with an algorithm that provides fully
 162 automatic cloud screening and instrument anomaly quality control (Giles et al., 2009). The version
 163 3 algorithm processing includes three quality levels. Level 1.0 data use the pre-field deployment
 164 sun calibration. Level 1.5 data use Level 1.0 data and apply cloud-screening and automatic quality
 165 control procedures. Data are raised to Level 2.0 after applying the final post-field deployment sun

166 calibration to Level 1.5 data. The Level 2 data is the most accurate, but it provides a longer delay
167 due to the requirement of post-field final calibration, so we used the Level 1.5 data, which is the
168 most accurate available. To determine the air quality near the ground, we used the PM_{2.5}
169 concentration data observed near the J-ALPS site. The Japanese Environment Ministry
170 consolidates the network of air pollution monitoring, including sulfur dioxide, nitrogen dioxide,
171 carbon monoxide, photochemical oxidants, suspended particulate matter, and PM_{2.5}, and provides
172 the monitoring value by the Atmospheric Environmental Regional Observation System (AEROS:
173 <http://soramame.taiki.go.jp/>). Since PM_{2.5} concentrations are not observed near all J-ALPS sites,
174 we used PM_{2.5} concentration data only near the three sites in Matsumoto, Suwa, and Ina.
175 Additionally, field observations were conducted in the Ina Basin on March 19 and 20, 2020, using
176 portable sun photometers, a PM_{2.5}, and a ceilometer. The Microtops-2 portable sun photometer is
177 easy to carry; it added to our fieldwork and provided AOT (Nakata et al. 2013; Sano et al., 2016).
178 We used a Microtops-2 photometer, calibrated with a standard Aerosol Robotics Network-Cimel
179 (AERONET-Cimel) radiometer. The P-Sensor PM_{2.5}, developed by the Nagoya University and
180 Panasonic Corporation, uses the light scattering method. In addition, we used a compact and
181 lightweight Vaisala ceilometer CL31, which can be used for cloud-base height and vertical
182 visibility measurements.
183

184 **3 Regional chemical transport model simulation: SCALE-Chem**

185 3.1 Model description

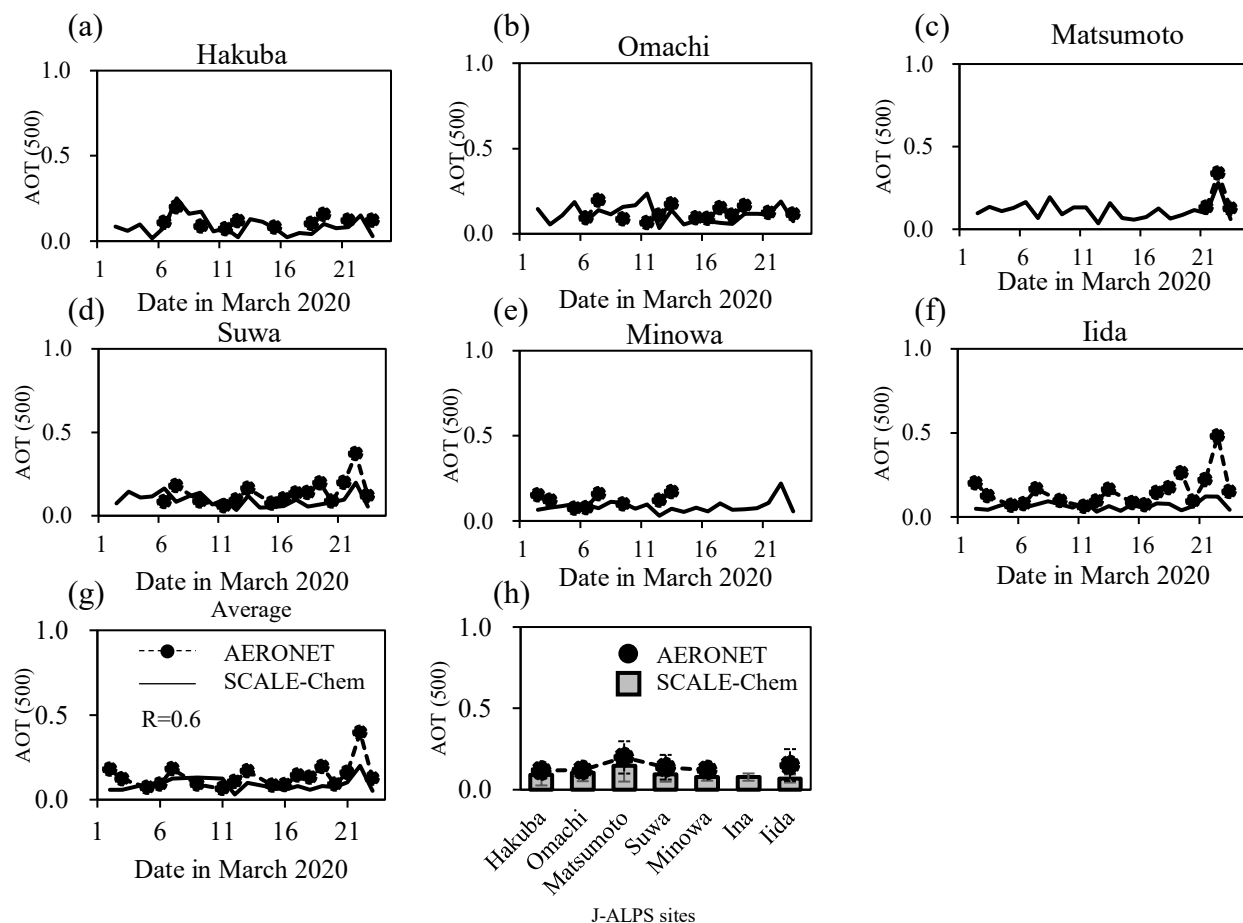
186 In this study, a regional chemical transport model simulation was conducted to investigate
187 the effects of terrain on aerosols. A chemical transport model (Kajino et al., 2019, 2021) was
188 implemented in the Scalable Computing for Advanced Library and Environment (SCALE)
189 meteorological model (Nishizawa et al., 2015; Sato et al., 2015). The chemical transport model
190 consists of advection, turbulent diffusion, gas-phase photochemistry, SOA chemistry, liquid-phase
191 chemistry, heterogeneous chemical reactions, and aerosol microphysical processes. The aerosol
192 microphysical processes include new particle formation, surface equilibrium vapor pressures of
193 organic and inorganic compounds, condensation and evaporation, Brownian coagulation, dry
194 deposition, grid-scale in-cloud scavenging, grid-scale below-cloud scavenging, sub-grid scale
195 convection and scavenging, and fog deposition processes. The aerosol categories are Aitken, soot-
196 free accumulation, accumulation internally mixed with soot, dust, and sea salt. The model
197 considers 12 tracers including two moments (0th (number) and 2nd (proportional to surface area))
198 and a mass of ten components (unidentified mass, or anthropogenic dust (UID), black carbon (BC),
199 organic mass (OM), mineral dust (MD), non-volatile components of sea salt (NS), SO₄²⁻, NO₃⁻,
200 NH₄⁺, Cl⁻, and H₂O) for each category. We used a chemical transport model coupled offline to
201 SCALE (SCALE-Chem). Offline coupling is a method in which a meteorological simulation is
202 first performed, and then the results are used to simulate chemical transport. A meteorological
203 simulation is required only once for an offline coupling model. Therefore, offline simulations are
204 computationally more efficient during sensitivity simulations (Kajino et al., 2019). Figure 1 shows
205 the simulation domain, which covers the central region of Japan with 92 × 92 horizontal grid cells
206 with a grid resolution of 5 km and 5 km in latitude and longitude, respectively. First, a
207 meteorological simulation was performed by SCALE. A mesoscale analysis (MANL) produced
208 by the Japan Meteorological Agency (JMA) was used for the initial and boundary conditions of
209 the SCALE. Surface heights based on GTOPO 30 from the United States Geological Survey The

210 target period was March 2020, and we simulated the period from March 1 to 23, including March
211 19 and 20, when we conducted on-site observations. A single run by SCALE started at 0:00
212 Coordinated Universal Time (UTC) on a date in the period and stopped after 30 h and 6 h from
213 the initial time was discarded as the spin-up (Inatsu et al., 2020). The boundary conditions for the
214 chemical transport model were built by serially connecting the outputs of the everyday runs.
215 REASv2 (Kurokawa et al. 2013) for anthropogenic emissions with monthly variations, and the
216 method of Li et al. (2017) was used for the hourly and vertical profiles of the emissions. We used
217 the monthly Global Fire Emissions Database (GFED3; Giglio et al. 2010) for open biomass
218 burning emissions and the Model of Emissions of Gases and Aerosols from Nature (MEGAN2;
219 Guenther et al.2006) for biogenic emissions. Hourly volcanic SO₂ emissions in Japan developed
220 by Kajino et al. (2021) were used. For the nesting boundary condition, we used the 3-D
221 concentration over the Asian region calculated by NHM-Chem with the same model domain
222 (covering East Asia with 30 km grid resolutions) and the same emission inventories as Kajino et
223 al. (2019). The simulated PM_{2.5} was derived as a proportion of the dry mass in which the
224 aerodynamic ambient (wet) diameter was smaller than 2.5 μm. The Mie theory calculation was
225 performed to derive the AOT at a wavelength of 500 nm using simulated log-normal size
226 distribution parameters and chemical compositions.

227 To investigate the terrain effects on aerosols around J-ALPS sites, three numerical
228 experiments, E1 (control experiment), E2 (E1 without topography), and E3 (E1 with removal all
229 anthropogenic emissions over Nagano prefecture), were evaluated. The differences between E1
230 and E2 represent the impact of topography on aerosols. For E2, the meteorological simulation was
231 performed without topography; that is, the region was flat. The same meteorological simulation
232 result from the SCALE was used for E1 and E3. Then, E1 minus E3 evaluated the local
233 anthropogenic emission effect on the aerosols.

234 3.2 Validation of the measurements

235 The simulation results of the E1-experiment by SCALE-Chem, described in the previous
236 section and abbreviated as E1 hereafter, were compared with observed AOT at J-ALPS sites.
237 Figure 2 presents the daily mean AOT (500) at a wavelength of 500 nm at six J-ALPS sites
238 (Hakuba, Omachi, Matsumoto, Suwa, Minowa, and Iida in Fig.2 (a) to Fig. (f), respectively). The
239 solid curve denotes the simulated results obtained using SCALE-Chem. The dots show AERONET
240 Level 1.5 data at the J-ALPS sites. It is clear from Fig. 2 that the amount of data varies from site
241 to site because the data acquisition period varies depending on the installation conditions of the
242 equipment and weather conditions. Sun photometry cannot obtain data on cloudy or rainy days.
243 For example, the Minowa site was unable to obtain data in the latter half of March, while the
244 Matsumoto site was only able to obtain data for the last few days of the target period. Further
245 observation data were not available at the Ina site in March 2020. Then, because the amount of
246 data was too small to examine the correlation between the model and observed data for each site,
247 six sites were averaged to examine the correlation of daily changes between the model simulations
248 and measurements (Fig.2 (g)). The daily average value of the AERONET data showed that AOT
249 (500) exceeding 0.3 was observed in Matsumoto, Suwa, and Iida on March 22, 2020, but no high
250 aerosol concentration event with AOT exceeding 0.5 was observed, indicating that the AOT (500)
251 at the J-ALPS site was low. A comparison of the average values for each site in Fig.2 (h) showed
252 that the AOT (500) values at Matsumoto tended to be the highest in the measurements and model
253 simulations. Figure 2 shows that the SCALE-Chem simulation results reproduce the AOT (500)
254 values observed at the AERONET/J-ALPS site.



255

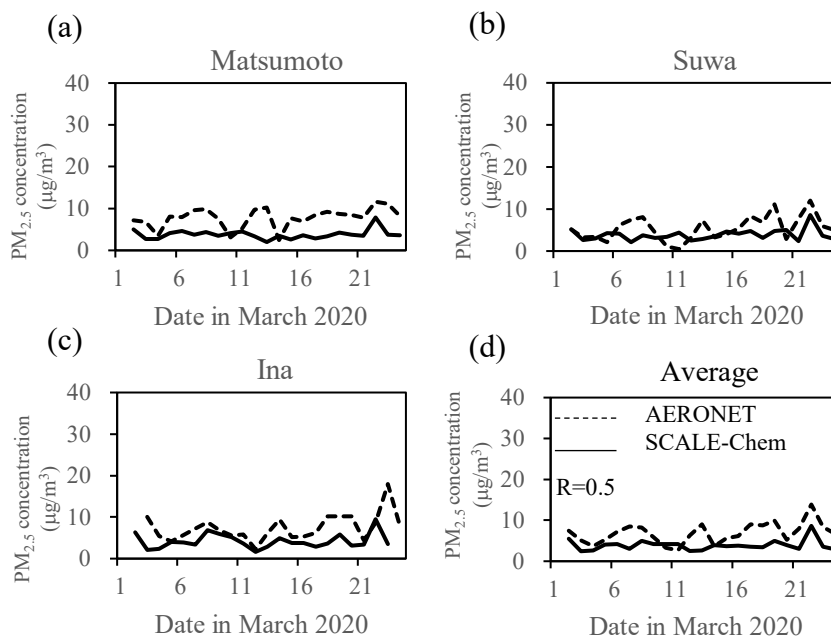
256 **Figure 2.** Daily mean AOT (500) at six J-ALPS sites as Hakuba, Omachi, Matsumoto, Suwa,
 257 Minowa, and Iida in Fig. (a) to Fig. (f), respectively. The solid curve denotes the simulated
 258 results by SCALE-Chem. The dots show AERONET Level 1.5 data at J-ALPS sites. Figs. (h)
 259 and (g) represent the AOT (500) values averaging over six sites and over the observation days,
 260 respectively.

261

262 Since AEROS observations of $PM_{2.5}$ concentrations were made near the Matsumoto, Suwa,
 263 and Ina sites of the J-ALPS, we compared the model results with the data shown in Fig. 3. The
 264 $PM_{2.5}$ concentrations were also not very high, but as with AOT, the trend of higher concentrations
 265 on March 22 was simulated in the model. The simulated concentrations at the three sites were
 266 underestimated, and this trend was more pronounced at the Matsumoto site. The Matsumoto site
 267 is located in the urban area of Matsumoto City, and there are potential problems with the
 268 uncertainty of the inventory and the spatial representativeness of the observation sites.

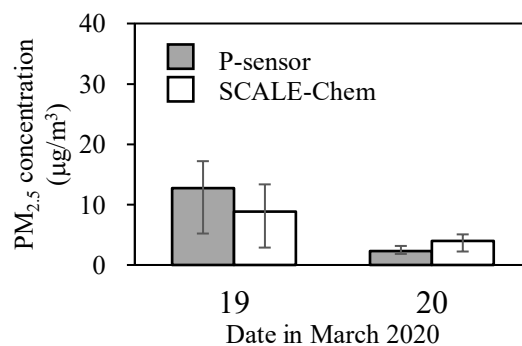
269 The results of observations in the Ina Basin using portable instruments were also compared
 270 with the model. The observation site is located between the Ina and Minowa sites and along the
 271 Tenryū River at ($N35.878^\circ$, $E137.988^\circ$) and at an altitude of 670 m. Observations were conducted
 272 at the site on March 19 and 20, 2020. The $PM_{2.5}$ concentration levels in the observed area were
 273 usually not too high, with an annual average value of $\sim 10 \mu\text{g}/\text{m}^3$. However, the morning of March
 274 19 showed higher than usual values of $PM_{2.5}$, whereas, on March 20, lower than usual values were

275 observed. Additional measurements were performed using portable sun photometers. The
 276 Microtops-2 instrument detected a high AOT on the morning of March 19 and a low AOT on
 277 March 20. These features were consistent with the ceilometer measurements. Notably, the
 278 ceilometer measured the vertical distribution of atmospheric aerosols. The measurements recorded
 279 on March 19, 2020, showed high concentrations of air pollutants in the morning. Figure 4 shows
 280 the comparison between the observation and simulated $PM_{2.5}$ concentrations. Both indicate that
 281 $PM_{2.5}$ concentrations were higher on the morning of March 19 than on the morning of March 20,
 282 and the observation and model values are almost the same. Comparisons between observation and
 283 simulation around J-ALPS sites indicate that the SCALE-Chem simulation could be used in further
 284 analyses of the impact of topography on aerosols.
 285



286
 287
 288
 289
 290
 291

Figure 3. Daily mean $PM_{2.5}$ at (a) Matsumoto, (b) Suwa, and (c) Ina sites and (d) average of 3 sites in March 2020. The dashed line indicates Atmospheric Environmental Regional Observation System (AEROS) data, and the solid line indicates SCALE-chem simulation.



292
 293
 294
 295

Figure 4. Observation $PM_{2.5}$ concentration and simulated $PM_{2.5}$ concentration by SCALE-Chem in the Ina basin on March 19 and 20, 2020, averaged from 06:00 to 10:00 local time. Error bars indicate the width of the maximum and the minimum values over average time.

296 **4 Feasible experiments using SCALE-Chem**

297 4.1 Mountain and local emission effects at J-ALPS sites

298 The mountain effects (*Mt effect*) on aerosols around J-ALPS sites could be investigated with the
 299 differences between the control experiment (E1) and the experiment without topography (E2) as:

300

$$301 \quad Mt \text{ effect} = (A_{E1} - A_{E2}) / A_{E1}, \quad (1)$$

302

303 where A_{Ex} indicates the value simulated by the experiment of Ex. Next, to evaluate the impact of
 304 aerosols originating from emissions in Nagano Prefecture, we compared an experiment in which
 305 emissions in Nagano Prefecture were eliminated (E3) with the control experiment (E1). This term
 306 will be used in this work to refer to the local emission effect (*local effect*).

307

$$308 \quad Local \text{ effect} = (A_{E1} - A_{E3}) / A_{E1}, \quad (2)$$

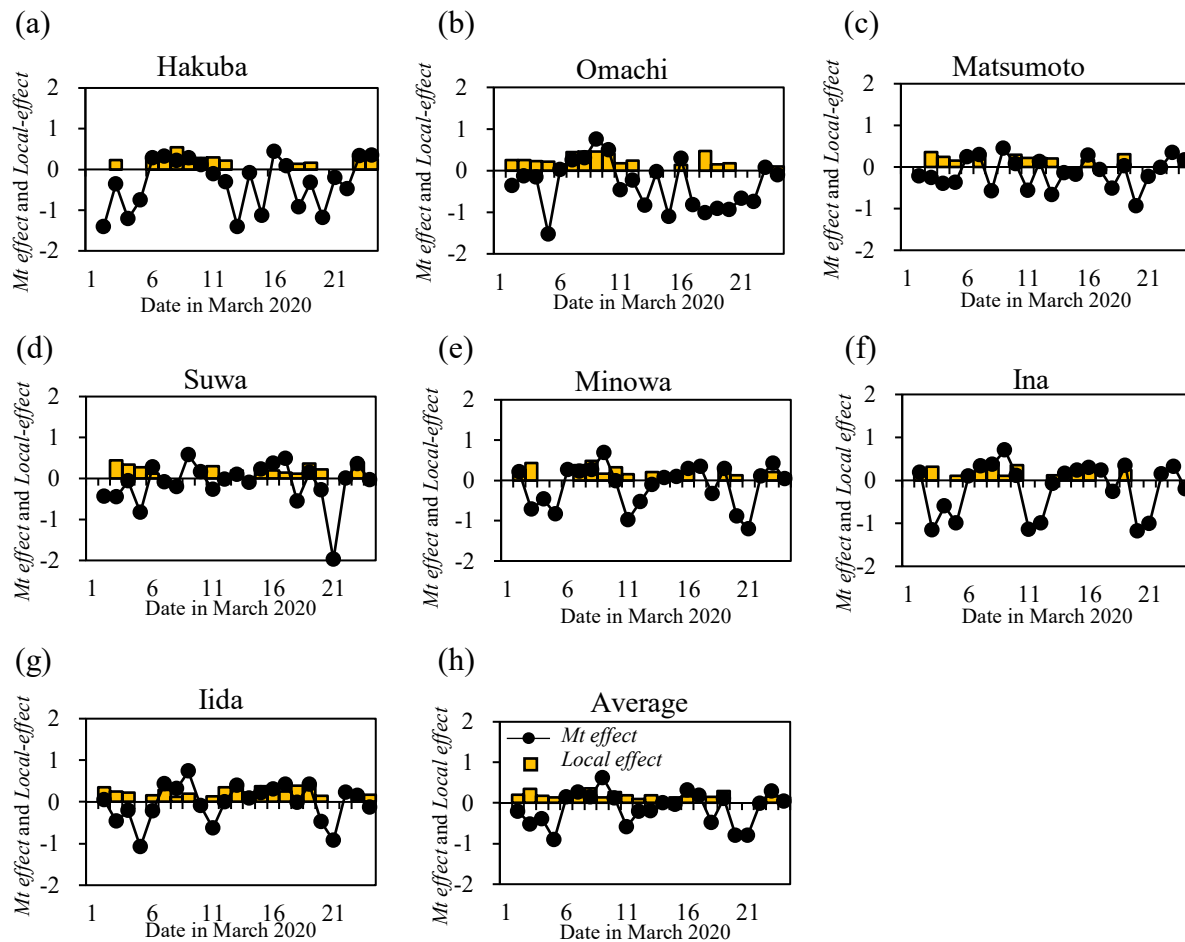
309

310 Figure 5 presents the daily change in the *Mt effect* (dotted line graph) and *local effect* (yellow bar
 311 graph) estimated from PM_{2.5} concentrations at J-ALPS sites. This clearly shows that the *Mt effect*
 312 is not always negative. That is to say, some days, the mountain reduces the aerosol concentrations,
 313 and some days, it increases them. Hakuba was the most northerly of the seven sites. Here, the rate
 314 of decrease in aerosol concentration due to the *Mt effect* was the greatest among the seven sites.
 315 On days when there is a significant decrease in concentration due to the *Mt effect*, the wind
 316 direction is often west to west-northwest. However, on days when aerosol concentrations are
 317 increasing due to the *Mt effect*, the *local effect* can be seen. In Omachi, which is located next to
 318 Hakuba to the north, the daily changes in the *Mt* and *local effects* are similar to those in Hakuba.
 319 It was observed that the southwest wind tended to dominate on days when the rate of decrease due
 320 to the *Mt effect* was high. In addition, as in Hakuba, the period of increased concentration due to
 321 the *Mt effect* in early March seems to correspond to the period when the *local effect* is large.
 322 Matsumoto has a smaller percentage of decrease in concentration due to the *Mt effect* than Hakuba
 323 and Omachi. Suwa shows similar daily changes in the *Mt effect* and *local effect* as Matsumoto.
 324 Minowa and Ina are geographically close, and the changes in the *Mt* and *local effects* are similar.
 325 Iida, the most southerly of the seven sites, shows similar daily changes in *Mt effect* as Minowa and
 326 Ina, but with a lower rate of decrease. The average of the seven sites shows that the rate of decrease
 327 in aerosol concentration due to the *Mt effect* is greater than the rate of increase in aerosol
 328 concentration due to the *Mt effect*. In addition, the *Mt effect* tends to have a positive value on the
 329 day when the *local effect* is more prominent. This suggests that on days when the aerosol
 330 concentration decreases due to the *Mt effect*, the effect of the mountains blocking the particles from
 331 outside the prefecture is significant. On the other hand, the days when the aerosol concentration
 332 increases due to the *Mt effect* are the days when air pollution caused by particles originating from
 333 sources within the prefecture is likely to occur, so it can be inferred that the terrain effect amplifies
 334 the concentration of particles originating from within the prefecture. The daily variation of the two
 335 effects suggests that, even on days when the *local effect* is substantial, the *Mt effect* has a negative
 336 value if the effect of stopping the inflow from outside the prefecture is greater than that of
 337 increasing PM_{2.5} concentration by the *local effect*.

338

339 As shown in Fig. 5, the *Mt effect* had a marked negative value on March 20 and a positive
 value on March 9. In the next section, using March 20 and 9 as examples, we will examine the

340 aerosol distribution on a day when advection from outside is blocked by mountains and a day when
 341 mountains increase the concentrations, respectively.
 342

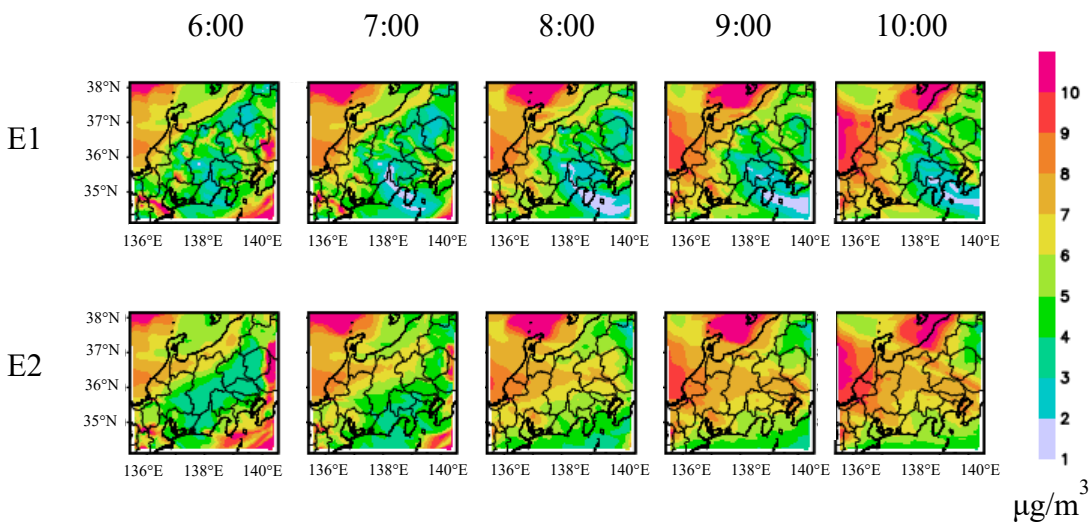


343
 344
 345
 346 **Figure 5.** Daily change of *Mt effect* (dots line graph) and *Local effect* (yellow bar graph)
 347 estimated from PM_{2.5} concentrations at J-ALPS sites in March 2020. The *Local effect* is a graph
 348 showing days when the value was greater than 0.1.

349 4.2 Mechanisms of the mountain effect on aerosols

350 First, the 20th of March, as shown in Fig. 4, was considered. Satellite observations and
 351 numerical model simulations show that aerosol concentrations are high from spring to summer
 352 over East Asia (Nakata et al., 2018). Spring is the season when aerosols from mainland China are
 353 especially likely to be transported to Japan (Nakata et al., 2015). Figure 6 shows the distribution
 354 of the PM_{2.5} concentration simulated by SCALE-Chem on March 20, from 6:00 to 10:00 local time.
 355 The upper figures represent the case of the E1 experiment and the lower E2 experiment.
 356 Transboundary pollution that had crossed the Sea of Japan was also observed. However, the PM_{2.5}
 357 concentrations were low around the J-ALPS sites on March 20. It can be seen that the PM_{2.5} air
 358 advection is blocked by the mountains. The results of E2, simulated without mountains, show that
 359 particles transported from the west also flow into Nagano Prefecture. Comparing the results of the

360 E1 and E2 simulations, it is clear that the mountain effect reduces air pollution in the vicinity of
 361 the J-ALPS site.
 362

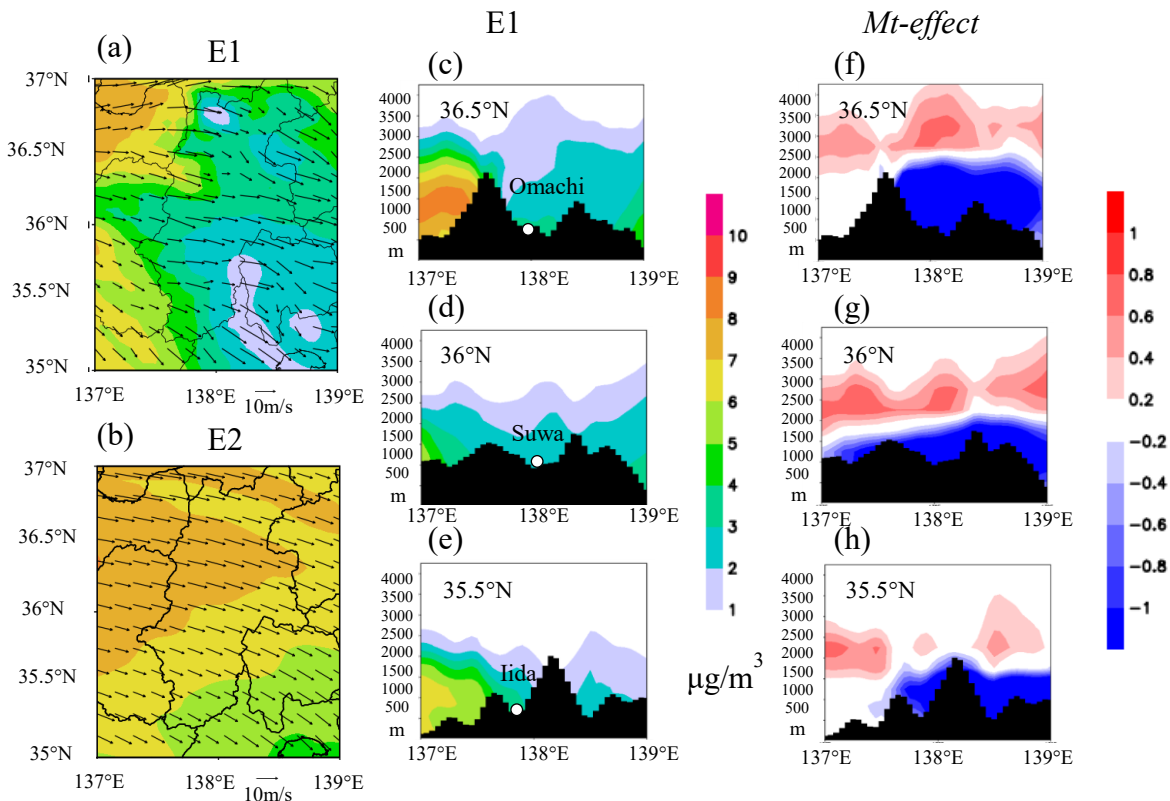


363
 364
 365 **Figure 6.** Distribution of $PM_{2.5}$ concentrations by SCALE-Chem from 06:00 to 10:00 local time
 366 on March 20, 2020. The upper and the lower figures represent the E1 and E2 experiments,
 367 respectively.
 368

369 Figure 7 (a) and (b) show the 2-dimensional distribution of $PM_{2.5}$ and wind vectors denoted
 370 by black arrows from SCALE-Chem simulations in two cases of experiment E1 and E2 over
 371 Nagano Prefecture. It is clear that the $PM_{2.5}$ concentrations (represented with the color scale)
 372 are higher in E2 than in E1. Figures 7(c), 7(d), and 7(e) show the vertical distribution of $PM_{2.5}$
 373 in a cross-sectional view in the east-west direction at 36.5° , 36° , and 35.5° N, respectively. This
 374 shows that aerosol particles are being held back by the mountains. On March 20, the prevailing
 375 wind was from the west, and we can assume that aerosol particles transported from this direction
 376 were blocked by mountains on the west side. To examine the extent to which $PM_{2.5}$ concentrations
 377 changed due to the effect of mountains, the east-west cross-sections of the mountain effect
 378 calculated by equation (1) are shown in Figs.7 (f)–(g). Near Omachi at 36.5° N, it is clear that
 379 aerosols are held back by the mountains to the west. In the vicinity of Suwa at 36° N, there is a
 380 chain of mountains to the west, although their elevation is lower than in the vicinity of Omachi,
 381 and it can be seen that these mountains are still capable of blocking aerosols. The Iida site is near
 382 35.5° N, and the elevation of the mountains on the west side is lower than that near 36.5° N;
 383 however, the effect of the mountains on the west side still reduces the aerosol concentration. In
 384 addition, the vertical cross-section shows that the aerosol concentration in the upper layer increases
 385 as the concentration in the lower layer decreases, owing to the mountain effect. On March 20, the
 386 air was clear when we observed it in the Ina Basin, but if the mountains were not effective in
 387 preventing aerosols from the outside, it is likely that the aerosol concentration would have
 388 increased due to transboundary pollution.
 389

390
 391
 392

393



394

395 **Figure 7.** Two-dimensional distribution of PM_{2.5} concentrations (presented with the color scale
 396 in the middle) and wind vectors (denoted by black arrows) from SCALE-Chem simulations in
 397 two cases of experiment (a) E1 and (b) E2. Figures (c), (d), and (e) present the vertical
 398 distribution of PM_{2.5} concentrations for experiment E1 in a cross-sectional view in the east-west
 399 direction at 36.5°N, 36°N, and 35.5°N, respectively. The *Mt effect* is shown in the right side
 400 figures (f), (g), and (h); scaled color is shown to the far right. Averaged from 06:00 to 10:00
 401 local time on March 20, 2020.

402

403

404

405

406

407

408

409

410

411

412

413

414

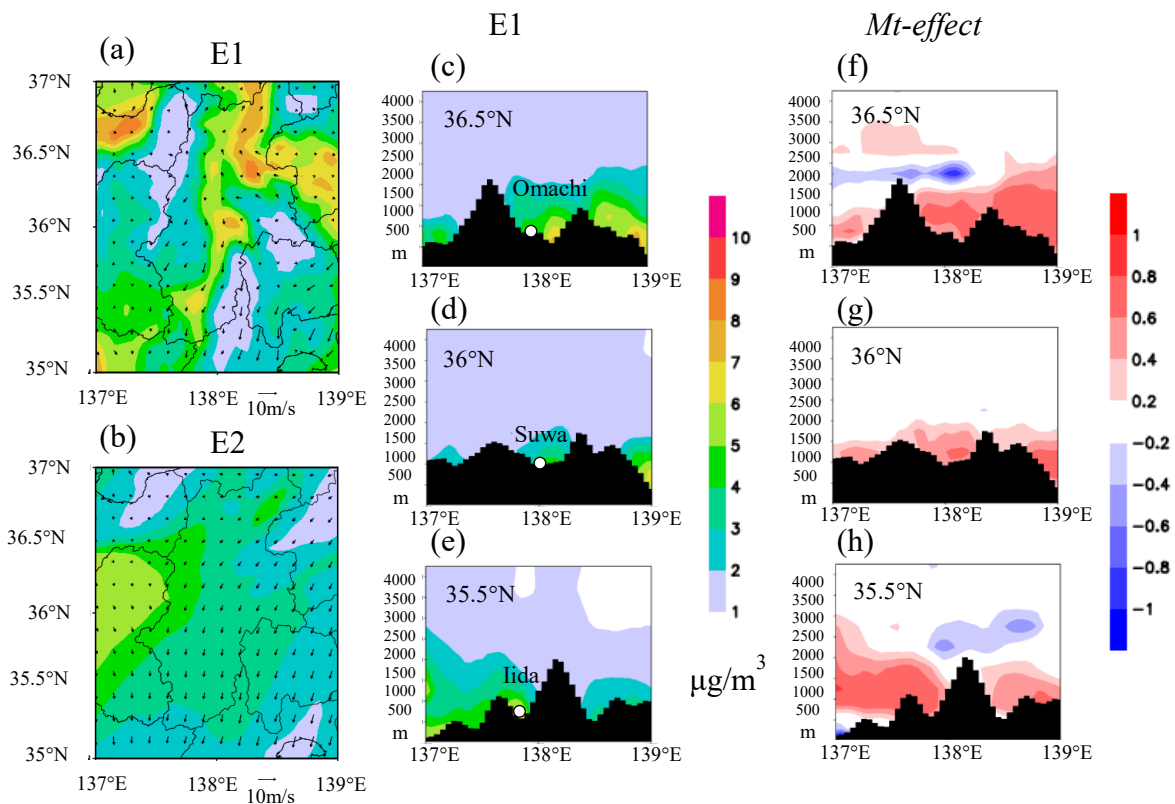
415

416

Below is a summary of the study results on the days when aerosol concentrations increased due to the *Mt effect*. March 9 was a day when the *Mt effect* was positive at all seven sites, as shown in Figure 5. Figures 8(a) and 8(b) show the PM_{2.5} concentration distribution and wind vectors around Nagano Prefecture on March 9 for the E1 and E2 simulations, as shown in Fig. 7. Compared with the case of March 20 shown in Fig. 7, Fig. 8 on March 9 indicates that the wind was weaker and the PM_{2.5} concentrations were higher in the basin. However, the simulation without topography showed that PM_{2.5} concentrations were uniformly distributed throughout Nagano Prefecture on March 9. This suggests that the concentrations were increasing in Nagano Prefecture due to topographical effects. The east-west cross-sectional view presented in Figs. 8(c)–(e) shows that the aerosol particle concentration was higher between the mountains. Figures 8 (f) to (g) present the concentration change due to the mountain effect. The *Mt effect* demonstrates an increase in aerosol concentration in the lower layer. Topographical effects have been shown to enhance air pollution in basins (Zhang et al., 2019). This is thought to be related to the fact that on days when the effect of local emissions is strong, the effect of mountains is positive. On days when

417 aerosol concentrations increase due to emission sources within the prefecture, the topographical
 418 effect of the basin reinforces the increase in concentrations over the J-ALPS sites. The vertical
 419 distribution of temperature at J-ALPS sites at 6:00 local time on March 9, when the aerosol
 420 concentration increased due to the positive *Mt effect*, is shown in Fig. 9. In the early morning of
 421 March 9, the ground was cooler, and a ground inversion layer formed. This is thought to have
 422 caused the aerosol concentration to rise because the atmosphere near the ground surface became
 423 stable, making it difficult for particles to diffuse in the upper layer. In the simulation without
 424 surrounding mountains (E2), the temperature near the ground was not as low as in the control
 425 simulation (E1), so the inversion layer was not as thick as in E1. This suggests that on days when
 426 the *Mt effect* is positive, the weather conditions are conducive to the accumulation of aerosols in
 427 the lower atmosphere. As can be seen from Fig. 5, there is a relationship between the positive *Mt*
 428 *effect* and *local effect*. The positive *Mt effect* increases the concentration of particles near the
 429 surface owing to the effect of topography. This effect is more pronounced when there is a *local*
 430 *effect*. On the other hand, if the inversion layer is caused by the topography effect, the particles
 431 brought from the outside will not increase the concentration near the surface. Therefore, there is
 432 no correlation between the *local effect* and the negative *Mt effect*. On March 19, when observations
 433 were made in the Ina Basin, atmospheric turbidity was observed in the morning, which is thought
 434 to have been caused by the positive *Mt effect*. The *Mt effect* was also positive on March 22, when
 435 the observed AOT and PM_{2.5} concentrations were high for the period, suggesting that the positive
 436 *Mt effect* may have accelerated the concentration increase.

437

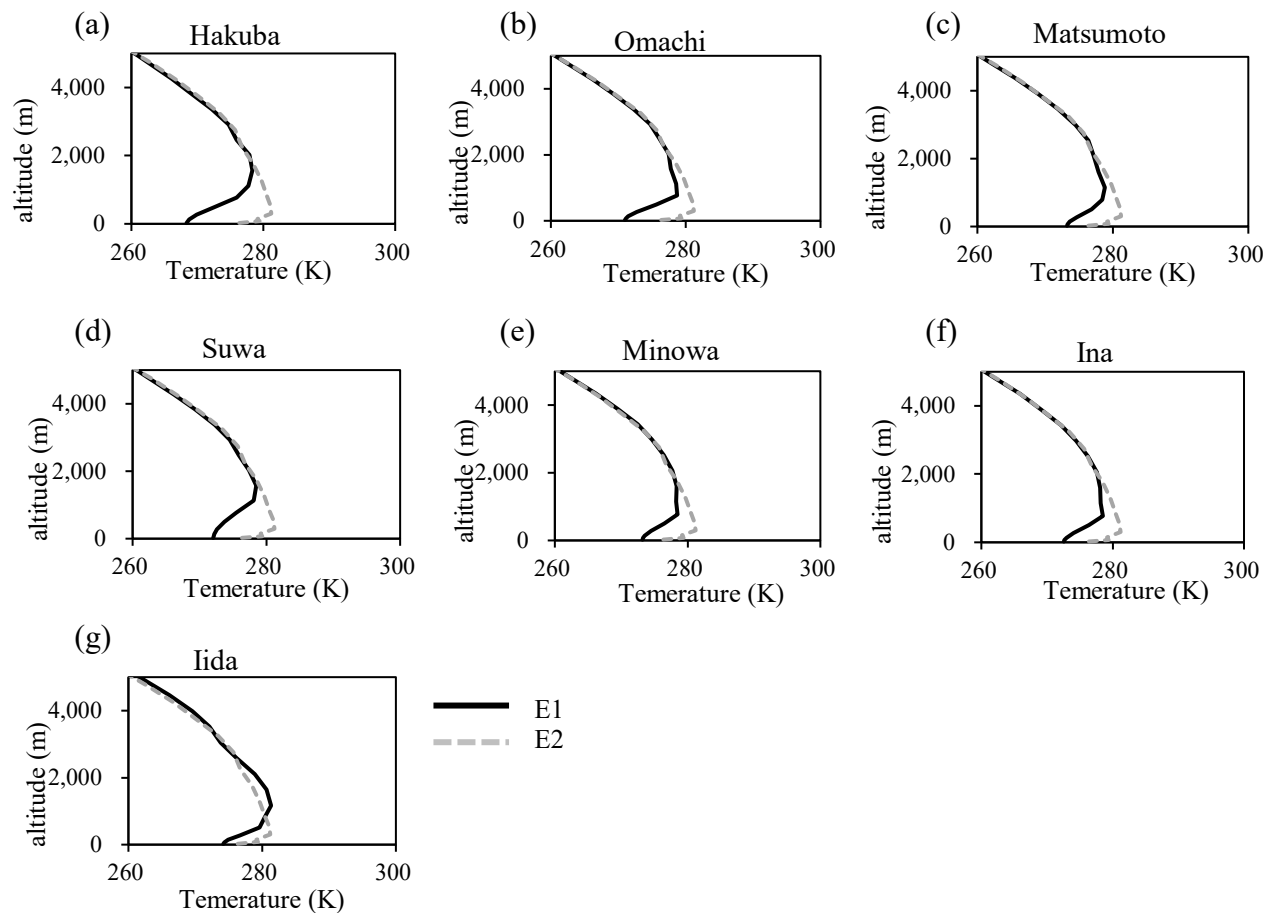


438

439 **Figure 8.** The same as Fig. 7, but for March 9, 2020.

440

441



442

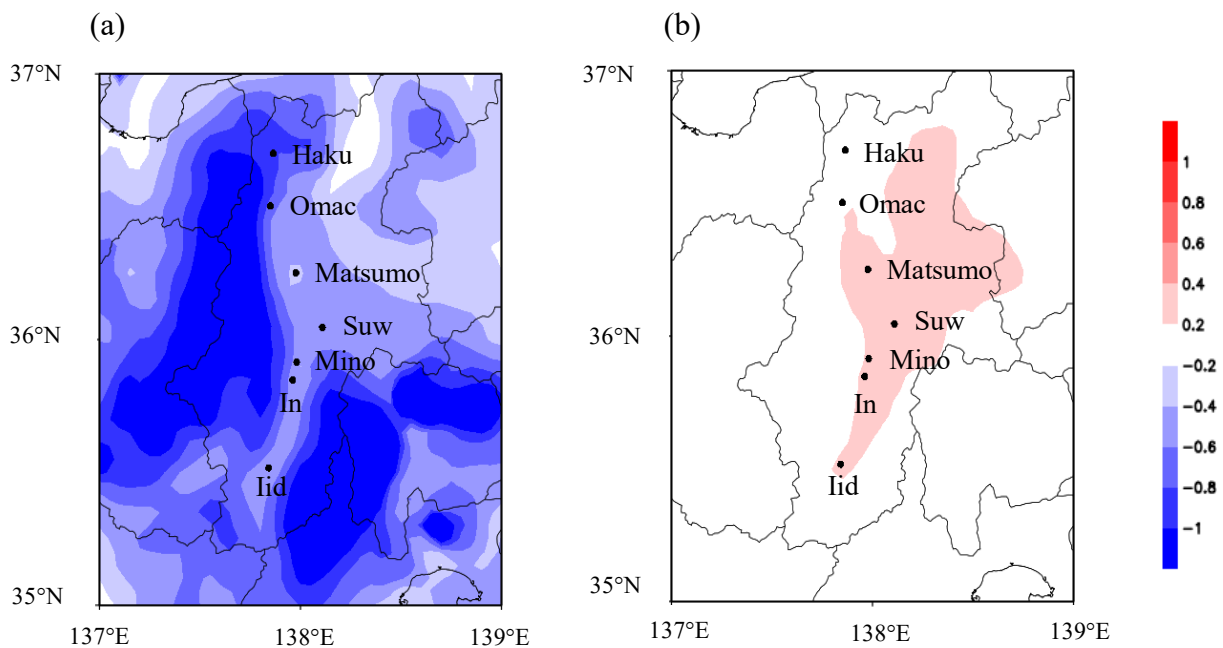
443

444 **Figure 9.** Vertical distribution of temperature at 06:00 local time on March 9, 2020, at (a) Hakuba,
 445 (b) Omachi, (c) Matsumoto, (d) Suwa, (e) Minowa, and (f) Iida sites simulated by SCALE-Chem
 446 for E1 and E2.

447 4.3 Simulation results over J-ALPS

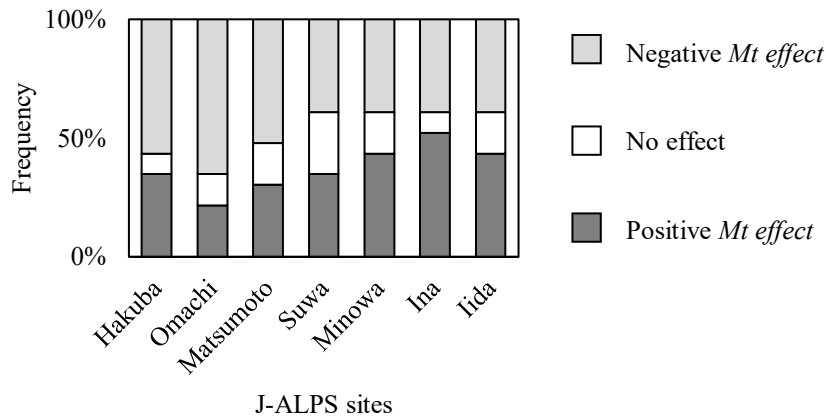
448 Figure 10 (a) shows the distribution of the *Mt effect* averaged during the simulation period,
 449 and it can be seen that the *Mt effect* is negative over the J-ALPS sites. Thus, it appears that
 450 mountains have a blocking effect on polluting particles from the outside. However, aerosol
 451 concentrations are not only reduced but sometimes increased by the presence of mountains. Figure
 452 10(b) shows the distribution of the *local effect* in Nagano Prefecture, and it can be seen that the
 453 distribution corresponds to the distribution of areas where the negative *Mt effect* is relatively small.
 454 The positive *Mt effect* on aerosol concentrations can also be described as the effect of increasing
 455 pollutant concentrations in basins. In areas where the *local effect* is large, the positive *Mt effect* is
 456 stronger. On days when there is no advection from outside the prefecture, and the increase in
 457 concentration due to emissions within the prefecture is dominant, the concentration will increase
 458 because of the positive *Mt effect*. Figure 10 shows the average for the period, so the negative *Mt*
 459 *effect* is lower in areas where the *local effect* is large. Negative and positive *Mt effects* are thought
 460 to occur simultaneously, but the averaged results indicate that the negative effect is significant.
 461 The simulation results show that the *Mt effect* blocking transboundary pollutant particles from

462 outside was greater than the enhancement of local air pollution due to the topographical effects
 463 over the J-ALPS sites in March 2020.
 464



465
 466
 467 **Figure 10.** Distribution of (a) *Mt effect* and (b) *Local effect* averaged during simulation period.
 468

469 To examine the frequency of days with negative and positive *Mt effects*, Fig. 11 shows the
 470 rate of occurrence days at each J-ALPS site. The days when the *Mt effect* reaches values greater
 471 than +0.1 are considered ‘positive *Mt effect*,’ those less than -0.1 ‘negative *Mt effect*,’ and others
 472 when the absolute value of the *Mt effect* is less than 0.1 are classified as having ‘no effect.’ As
 473 shown in Fig. 11, Hakuba, Omachi, and Matsumoto, in the northern part of the J-ALPS sites, have
 474 a negative *Mt effect* rate higher than 50%. In other words, mountains blocked the aerosol particles
 475 more than half the time. In March, transboundary pollution aerosols were transported from
 476 mainland China. This area has high mountains to the west, and hence, the pollutant aerosols seem
 477 to be blocked by the *Mt effect*. On the other hand, Iida, Ina, and Minowa, which are located in the
 478 southern part of the sites, tended to have a higher percentage of days with a positive *Mt effect*.
 479



480

481 **Figure 11.** Frequency of days with positive *Mt effect* and days with negative *Mt effect* during
 482 simulation period at each site.

483

484

485

486

487

488

489

490

491

492

493

494

495

496

497

498

499

500

501

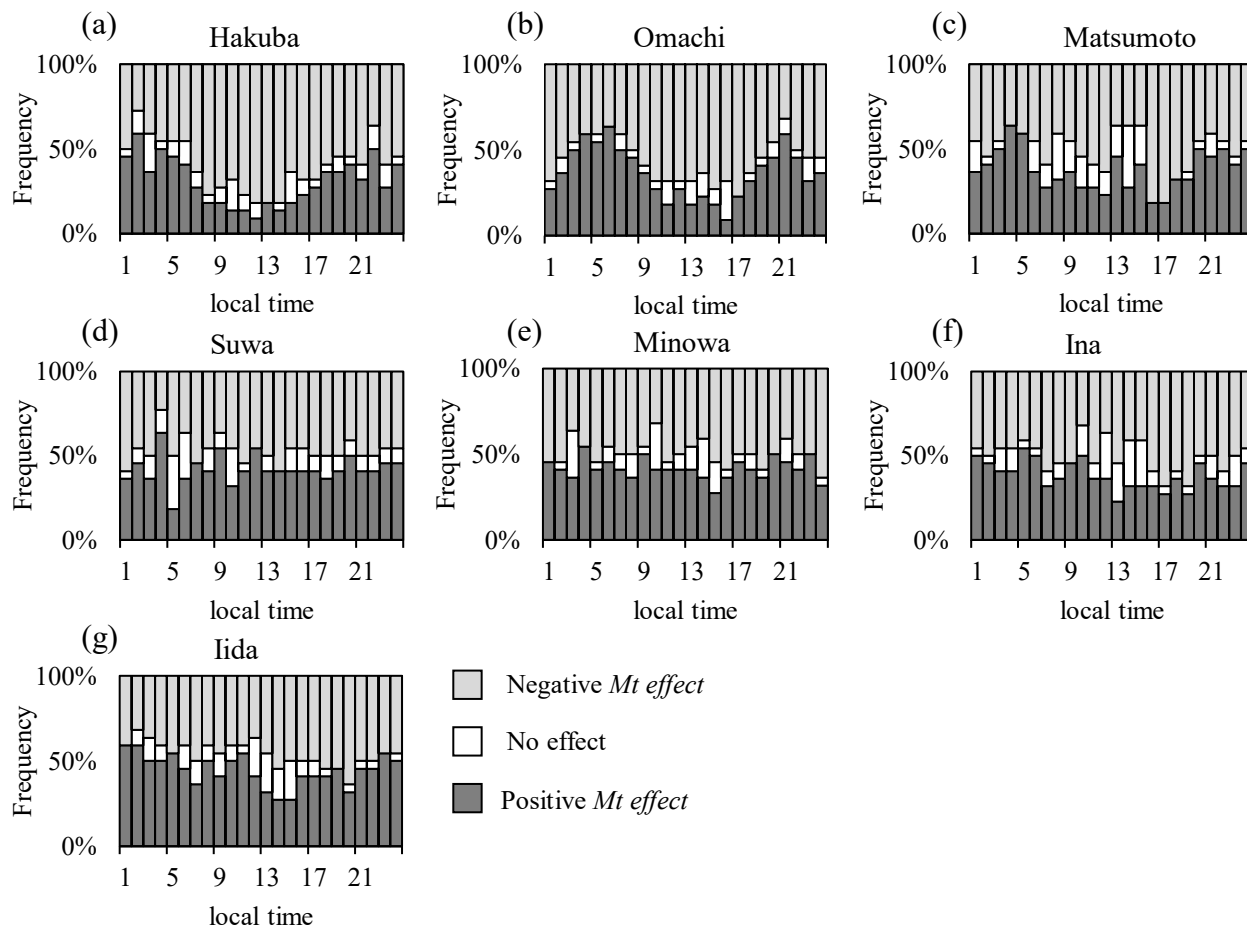
502

503

504

Figure 12 shows the relative daily frequency of the positive and negative *Mt effects* at each J-ALPS site in March 2020. The sunrise and sunset are around 6:00 and 18:00, respectively, at a local time in March in Nagano Prefecture. In Hakuba, there is a distinct diurnal variation in which a positive *Mt effect* is more likely to occur before sunrise and at night, and the frequency of positive *Mt effect* is lower during the day. During the hours when a positive *Mt effect* is more likely to occur, the frequency of negative *Mt effect* is relatively lower, but the percentage of negative *Mt effect* occurring throughout the day is high, reaching approximately 80% during the day. In Omachi, the frequency of the *Mt effect* showed diurnal variation, with a higher percentage of positive *Mt effect* occurring around sunrise and at night. However, during other times of the day, the percentage of the negative *Mt effect* was high. In Matsumoto, the percentage of the *Mt effect* was also high, but the percentage of the positive *Mt effect* tended to be higher around sunrise and at night. In Suwa and Minowa, there was no apparent diurnal variation, but the highest percentage of positive *Mt effect* was observed at 04:00. In Ina and Iida, the percentage of the positive *Mt effect* tends to be higher in the early morning than in the daytime. At the J-ALPS site, a negative *Mt effect* dominates at all times of day, but a positive *Mt effect* tends to happen in the early morning when an inversion layer is more likely to occur.

It was found that mountains have a two-way effect, preventing advection from the outside and trapping air masses in the basin surrounded by mountains. The effects are greater depending on the meteorological conditions, the presence or absence of external transboundary pollution, and the level of local emissions.



505

506 **Figure 12** Time variation of frequency in positive Mt effect and negative Mt effect during
 507 simulation period at each site.

508

509 **5 Conclusions**

510 To investigate the effect of mountain topography on aerosols, intensive DRAGON/J-ALPS
 511 observations were conducted around Nagano Prefecture, Japan. High concentrations of aerosol
 512 pollution were not observed in March 2020. To interpret the measurements of DRAGON/J-ALPS,
 513 three types of simulation experiments were carried out using a regional chemical transport model,
 514 SCALE-Chem. One was the control simulation, the second was the simulation without topography,
 515 and the third was the simulation eliminating local emissions in Nagano Prefecture. From the results
 516 of these simulations, we estimated the Mt and *local effects* in Nagano Prefecture. The presence of
 517 mountains was found to increase or decrease aerosol concentration in some cases. However, when
 518 averaged over the simulation period, the results show that the Mt effect effectively reduces aerosol
 519 concentrations. On the days when aerosol concentrations increased due to the Mt effect,
 520 meteorological conditions with high local emissions and the basin effect acted synergistically to
 521 accelerate the increase in aerosol concentrations. This trend was more pronounced in the southern
 522 region of the J-ALPS. However, at all sites, the aerosol inflow was blocked by mountains located
 523 to the west.

524 In Japan, spring is the season when transboundary pollution from mainland China is most
525 likely to be observed, but the aerosols from outside were suppressed at the J-ALPS sites because
526 they are surrounded by high mountains. Therefore, even on days when transboundary pollution
527 was observed in other parts of Japan, the aerosol concentrations were not very high at the J-ALPS
528 sites. In future work, we would like to investigate the seasonal variation of the mountain effect
529 using the data observed from seasons other than spring. Furthermore, the magnitude of
530 transboundary pollution, advection height, and the influence of meteorological conditions should
531 be taken into account, along with topographical effects.
532

533 **Acknowledgments**

534 The authors would like to thank Dr. Brent Holben & NASA/AERONET group, and Prof. Itaru
535 Sano and local organization members of J-ALPS. This study was supported in part by the Global
536 Change Observation Mission - Climate project by JAXA (no. JX-PSPC – 524344 & 530188), JSPS
537 KAKENHI Grant Number 19h04242. Yousuke Sato was supported by the Research Field of
538 Hokkaido Weather Forecast and Technology Development (Hokkaido Weather Technology Center
539 Co. Ltd.). SCALE was developed by Team-SCALE of RIKEN (<https://scale.riken.jp/>). The
540 SCALE source code is downloadable from the SCALE website (<https://scale.riken.jp/>). The
541 chemical model part of SCALE-Chem is subject to a license agreement with the Japan
542 Meteorological Agency. Further information is available at [https://www.mri-](https://www.mri-jma.go.jp/Dep/glb/nhmchem_model/application_en.html)
543 [jma.go.jp/Dep/glb/nhmchem_model/application_en.html](https://www.mri-jma.go.jp/Dep/glb/nhmchem_model/application_en.html). The AOT data at the J-ALPS site are
544 available at AERONET via <https://aeronet.gsfc.nasa.gov/>). The PM_{2.5} data used in this study are
545 available at AEROS via (<http://soramame.taiki.go.jp/>).

546 **References**

- 547 Aikawa, M., Ohara, T., Hiraki, T., Oishi, O., Tsuji, A., Yamagami, M., et al. (2010), Significant
548 geographic gradients in particulate sulfate over Japan determined from multiple-site
549 measurements and a chemical transport model: Impacts of transboundary pollution from the
550 Asian continent. *Atmospheric Environment*, 44(3), 381–391,
551 doi:10.1016/j.atmosenv.2009.10.025.
552
- 553 Chang, Y.S., Carmichael, G. R., Kurita, H., & Ueda, H. (1989), The transport and formation of
554 photochemical oxidants in central Japan. *Atmospheric Environment*, 23(2), 363–393.
555
- 556 Chuang, M., Chiang, P., Chan, C., Wang, C., Chang, E., & Lee, C. (2008), Elevated 3D
557 structures of PM_{2.5} and impact of complex terrain-forcing circulations on heavy haze pollution
558 over Sichuan Basin, China. *Science of the Total Environment*, 399, 128–146.
559
- 560 Diémoz, H., Barnaba, F., Magri, T., Pession, G., Dionisi, D., Pittavino, S., et al. (2019),
561 Transport of Po Valley aerosol pollution to the northwestern Alps –Part 1: Phenomenology.
562 *Atmospheric Chemistry and Physics*, 19, 3065–3095, <https://doi.org/10.5194/acp-19-3065-2019>.
563
- 564 Giglio, L., Randerson, J. T., van der Werf, G. R., Kasibhatla, P. S., Collatz, G. J., Morton, D. C.
565 & DeFries, R. S. (2010), Assessing variability and long-term trends in burned area by merging
566 multiple satellite fire products, *Biogeosciences*, 7, 1171–1186.
567

- 568 Giles, D. M., Sinyuk, A., Sorokin, M. G., Schafer, J. S., Smirnov, A., Slutsker, I., et al. (2019),
569 Advancements in the Aerosol Robotic Network (AERONET) Version 3 database – automated
570 near-real-time quality control algorithm with improved cloud screening for Sun photometer
571 aerosol optical depth (AOD) measurements. *Atmospheric Measurement Techniques*, *12*, 169–
572 209, <https://doi.org/10.5194/amt-12-169-2019>.
573
- 574 Guenther, A., Karl, T., Harley, P., Wiedinmyer, C., Palmer, P. I., & Geron, C. (2006), Estimates
575 of global terrestrial isoprene emissions using MEGAN (Model of Emissions of Gases and
576 Aerosols from Nature). *Atmospheric Chemistry and Physics*, *6*, 3181–3210.
577
- 578 Holben, B.N., Eck, T.F, Slutsker, I., Tanré, D., Buis, J.P., Setzer, A., et al. (1998), AERONET -
579 A federated instrumentnetwork and data archive for aerosol characterization. *Remote Sensing of*
580 *Environment*, *66*, 1–16.
581
- 582 Holben, B. N., Kim, J., Sano, I., Mukai, S., Eck, T. F., Giles, D. M., et al. (2018), An overview
583 of meso-scale aerosol processes, comparison and validation studies from DRAGON networks.
584 *Atmospheric Chemistry and Physics*, *18* (2), 655–671.
585
- 586 Hu, W., Zhao, T., Bai, Y., Shen, L., Sun, X., & Gu, Y. (2020), Contribution of regional PM_{2.5}
587 transport to air pollution enhanced by sub-basin topography: A modeling case over Central
588 China. *Atmosphere*, *11*(11), 1258, <https://doi.org/10.3390/atmos11111258>.
589
- 590 Inatsu, M., Tanji, S., & Sato, Y. (2020), Toward predicting expressway closures due to blowing
591 snow events. *Cold Regions Science and Technology*, *177*, 103123.
592
- 593 IPCC (Intergovernmental panel on climate change) (2013), *Climate change: The Physical*
594 *Science Basis, Contribution of Working Group 1 to the Fifth Assessment Report of the IPCC*,
595 Cambridge University Press, Cambridge.
596
- 597 Kajino, M., Deushi, M., Sekiyama, T.T., Oshima, N., Yumimoto, K., Tanaka, T.Y., et al. (2019),
598 NHM-Chem, the Japan meteorological agency’s regional meteorology – chemistry model:
599 Model evaluations toward the consistent predictions of the chemical, physical, and optical
600 properties of aerosols. *Journal of the Meteorological Society of Japan*, *97*(2), 337–374.
601
- 602 Kajino, M., Deushi, M., Sekiyama, T. T., Oshima, N., Yumimoto, K., Tanaka, T. Y., et al.
603 (2021), Comparison of three aerosol representations of NHM-Chem (v1.0) for the simulations of
604 air quality and climate-relevant variables. *Geoscientific Model Development*,
605 <https://doi.org/10.5194/gmd-14-2235-2021>.
606
- 607 Kaneyasu, N., Yamamoto, S., Sato, K., Takami, A., Hayashi, M., Hara, K., et al. (2014), Impact
608 of long-range transport of aerosols on the PM_{2.5} composition at a major metropolitan area in the
609 northern Kyushu area of Japan. *Atmospheric Environment*, *97*, 416–425,
610 [doi:10.1016/J.ATMOENV.2014.01.029](https://doi.org/10.1016/J.ATMOENV.2014.01.029).
611
- 612 Kurokawa, J., Ohara, T., Morikawa, T., Hanayama, S., Janssens-Maenhout, G., Fukui, T., et al.
613 (2013), Emissions of air pollutants and greenhouse gases over Asian regions during 2000–2008:

- 614 Regional Emission inventory in Asia (REAS) version 2. *Atmospheric Chemistry and Physics*, 13,
615 11019–11058.
- 616
- 617 Li, M., Zhang, Q., Kurokawa, J., Woo, J.-H., He, K., Lu, Z., et al. (2017), MIX: A mosaic Asian
618 anthropogenic emission inventory under the international collaboration framework of the MICS-
619 Asia and HTAP. *Atmospheric Chemistry and Physics*, 17, 935–963.
- 620
- 621 Nakata, M., Sano, I., Mukai, S., & Holben, B. N. (2013), Spatial and Temporal Variations of
622 Atmospheric Aerosol in Osaka. *Atmosphere*, 4(2), 157–168, doi:10.3390/atmos4020157.
- 623
- 624 Nakata, M., Sano, I., & Mukai, S. (2015), Air Pollutants in Osaka (Japan). *Frontiers in*
625 *Environmental Science*, 3, 18, doi: 10.3389 /fenvs.2015.00018.
- 626
- 627 Nakata, M., Mukai, S., & Yasumoto, M. (2018), Seasonal and regional characteristics of aerosol
628 pollution in East and Southeast Asia. *Frontiers in Environmental Science*, 6, 29,
629 <https://doi.org/10.3389/fenvs.2018.00029>.
- 630
- 631 Nishizawa, S., Yashiro, H., Sato, Y., Miyamoto, Y., & Tomita, H. (2015), Influence of grid
632 aspect ratio on planetary boundary layer turbulence in large-eddy simulations. *Geoscientific*
633 *Model Development*, 28, 8(10), 3393–341.
- 634
- 635 Togashi, H. (2001), Geomorphology and geology of Nagano prefecture. *Bulletin of Nagano*
636 *Nature Conservation Research Institute*, 4(1), 1–9 (in Japanese).
- 637
- 638 Sano, I., Mukai, S., Nakata, M., & Holben, B. N. (2016), Regional and local variations in
639 atmospheric aerosols using ground-based sun photometry during distributed regional aerosol
640 gridded observation networks (DRAGON) in 2012. *Atmospheric Chemistry and Physics*, 16,
641 14795–14803, doi:10.5194/acp-16-14795-2016.
- 642
- 643 Sasaki, K., Kurita, H., Carmichael, G. R., Chang, Y. S., Murano, K., & Ueda, H. (1988),
644 Behavior of sulfate, nitrate and other pollutants in the long-range transport of air pollution.
645 *Atmospheric Environment*, 22(7), 1301–1308.
- 646
- 647 Sato, Y., Nishizawa, S., Yashiro, H., Miyamoto, Y., Kajikawa, Y., & Tomita, H. (2015), Impacts
648 of cloud microphysics on trade wind cumulus: which cloud microphysics processes contribute to
649 the diversity in a large eddy simulation? *Progress in Earth and Planetary Science*, 2(1), 23,
650 doi:10.1186/s40645-015-0053-6.
- 651
- 652 Snider, G., Weagle, C. L., Murdymootoo, K. K., Ring, A., Ritchie, Y., Stone, E., et al. (2016),
653 Variation in global chemical composition of PM_{2.5}: emerging results from SPARTAN.
654 *Atmospheric Chemistry and Physics*, 16, 9629–9653, doi:10.5194/acp-16-9629-2016.
- 655
- 656 Su, B., Li, H., Zhang, M., Bilar, M., Wang, M., Atique, L., et al. (2020), Optical and physical
657 characteristics of aerosol vertical layers over Northeastern China. *Atmosphere*, 11, 501.
- 658

659 Van Donkelaar, A., Martin, R. V, Brauer, M., & Boys, B. L. (2015), Use of satellite observations
660 for long-term exposure assessment of global concentrations of fine particulate matter.
661 *Environmental Health Perspectives*, *123*, 135–143, doi:10.1289/ehp.1408646.

662
663 Zhang, Z., Xu, X., Qiao, L., Gong, D., Kim, S. J., Wang, Y., & Mao, R. (2018), Numerical
664 simulations of the effects of regional topography on haze pollution in Beijing. *Scientific Reports*,
665 *8*, 5504.

666
667 Zhang, L. Guo, X. Zhao, T., Gong, S., Xu, X., Li, Y., et al. (2019), A modelling study of the
668 terrain effects on haze pollution in the Sichuan Basin, *Atmospheric Environment*, *196*, 77-85.
669

670

671